

Design and Evaluation of a Novel Antenna Array for Azimuthal Angle-of-Arrival Measurement

Steven W. Ellingson, *Member, IEEE*

Abstract—This paper describes a novel antenna array concept in which a “Y”-shaped distribution of elements is used to achieve uniform angle-of-arrival (AOA) measurement performance in azimuth, and a ground plane is employed to reduce the potential for confusion due to scattering from nearby structures and interference from low elevation angles. A simple method for field calibration of this array is also presented. A prototype has been built and tested in field conditions at 460 MHz. Using maximum likelihood estimation, the array is able to resolve single AOAs to within a few degrees and is able to identify discrete multipath from the same source. A shortcoming of the field-tested design is that it has poor gain along the horizon, due to edge diffraction from the ground plane. To control this diffraction, an elliptical rolled edge termination is proposed. It is shown that a rolled edge increases the horizon gain by 5 dB while maintaining high suppression at low elevations and maintaining a low physical profile.

Index Terms—Angle-of-arrival estimation, antenna arrays, UHF measurements.

I. INTRODUCTION

A PROBLEM OF current interest to the terrestrial mobile radio community is how to accurately measure the angle-of-arrival (AOA) of signals received at a base station due to a mobile user in communication with that base station. Applications include “smart antenna” processing ([1] and its references), cellular site planning and channel modeling ([2] and references), and various location-based services such as wireless E-911 and location-specific billing ([3] and references). A key element in the design of many AOA measurement systems is, of course, an antenna array. Not much effort has been reported on the development of antenna arrays which are tailored to this problem. Instead, most of the emphasis has been devoted to antenna arrays which are simple to analyze or can be implemented on existing tower structures. For traditional cellular base stations, this usually means linear arrays covering 120° azimuthal sectors. Examples of AOA measurement systems developed for these conditions are reported in [4] and [5].

However, there are many cases in which legacy antenna system design is not a restriction. For example, base station antenna systems are often installed on building rooftops, where there may be some flexibility in the placement of the elements. Also, it is common for commercial, government, and military

applications to use temporary, vehicle-mounted base stations, which may allow some flexibility in array design. New towers can be designed from the outset using new antenna array concepts. Finally, any new system which is designed for AOA measurement may be able to take advantage of alternative array concepts.

This paper describes a novel antenna array concept which may be helpful in these applications. This design uses a “Y”-shaped distribution of elements to achieve uniform coverage in the azimuthal plane. The elements are implemented as vertically polarized quarter-wave monopoles mounted on top of a ground plane. The presence of the ground plane reduces the sensitivity of the array to energy scattered from the mounting structure (assumed to be below the array) and nearby objects. A simple method for field calibration of this array has been developed. A prototype of this array has been built and tested in field conditions at 460 MHz, with good results. A shortcoming of this design is that it has poor gain along the horizon, due to diffraction from the edge of the ground plane. To control this diffraction, an elliptical rolled edge termination is proposed. Using a rolled edge, the horizon gain of a vertical monopole on finite ground plane can be increased by 5 dB while maintaining high suppression at low elevations. Taking the array factor into account, such arrays can achieve gain comparable to the stacked dipole configurations traditionally used at base stations. Furthermore, this performance can be achieved in an antenna system which is about one wavelength in height, including the rolled edge.

This paper is organized as follows. Section II outlines some theory relevant to the problem of AOA estimation. In Section III, four geometries—the linear array, the circular array, the “L”-shaped array, and the “Y”-shaped array—are considered in terms of their performance and cost effectiveness for azimuthal AOA estimation. The “Y” is shown to have some compelling advantages over the other geometries. In Section IV, the elevation plane performance is considered. The patterns of the untreated and rolled edge versions of the array are analyzed and compared. In Section V, the mutual coupling among elements in the “Y” array is analyzed, and a technique for dealing with the coupling in AOA estimation is proposed. Section VI presents some AOA estimation results obtained from a field study in which an untreated-edge version of the proposed array was used for azimuthal AOA estimation at 460 MHz.

II. AOA ESTIMATION

Consider an antenna array consisting of N identical elements, with each element having a pattern which, in the absence of the other elements, is isotropic in azimuth. Let us further assume

Manuscript received March 10, 2000; revised December 11, 2000. This work was supported in part by the National Science Foundation under Grant ANI-9809018, the SETI Institute, and the Ohio State University.

The author is with The Ohio State University ElectroScience Laboratory, Department of Electrical Engineering, Columbus, OH 43212 USA (e-mail: ellingson@ieee.org).

Publisher Item Identifier S 0018-926X(01)05254-1.

that the narrowband assumption applies. That is, any signals incident on the array are assumed to have bandwidth sufficiently small such that the array response can be accurately described in terms of gains and phase shifts, as opposed to gains and time delays. For a single narrowband signal $s(t)$ incident on this array from angle ϕ at time t , the complex baseband outputs are given by $\mathbf{x}(t) = [x_1(t)x_2(t)\cdots x_N(t)]^T$ where

$$\mathbf{x}(t) = \mathbf{Z}^{-1}\mathbf{a}(\phi)s(t) + \mathbf{n}(t). \quad (1)$$

In this model, $\mathbf{a}(\phi)$ is an $N \times 1$ “steering vector” which describes the voltages induced on each element by the incident signal in the absence of the other elements, i.e., neglecting the mutual coupling between the elements. \mathbf{Z} is approximated as the $N \times N$ open-circuit impedance matrix, in this case normalized to a unitless symmetric matrix that describes the coupling. Thus, $\mathbf{Z}^{-1}\mathbf{a}(\phi)$ is proportional to the currents at the terminals of each element in the array, assuming equal load impedances. Finally, $\mathbf{n}(t)$ is an $N \times 1$ vector representing the noise present in the data, which is assumed to be thermal in nature, and thus is well-modeled as complex circular Gaussian white noise which is identically distributed and uncorrelated between elements.

In the more general case where power is incident on the array from M discrete directions, the model can be compactly expressed as

$$\mathbf{x}(t) = \mathbf{Z}^{-1}\mathbf{A}(\Phi)\mathbf{s}(t) + \mathbf{n}(t) \quad (2)$$

where $\mathbf{A}(\Phi)$ is an $N \times M$ matrix composed of M steering vectors associated with the incident AOAs, $\Phi = \{\phi_1, \phi_2, \dots, \phi_M\}$, and $\mathbf{s}(t) = [s_1(t)s_2(t)\cdots s_M(t)]^T$. To be concise, let us also define the *response vector* $\mathbf{b}(\phi) = \mathbf{Z}^{-1}\mathbf{a}(\phi)$ and similarly $\mathbf{B}(\Phi) = \mathbf{Z}^{-1}\mathbf{A}(\Phi)$.

In this study, the maximum likelihood (ML) method of Ziskind and Wax [6] is used to estimate Φ . In this method, one performs an M -dimensional search for the set of AOAs which maximizes the likelihood function derived from the above model. This estimator is given by

$$\arg \max_{\Phi} \text{Tr}\{\mathbf{P}_{\mathbf{B}(\Phi)}\mathbf{R}\} \quad (3)$$

where \mathbf{R} is the spatial covariance matrix, defined as the expected value of the outer product $\mathbf{x}(t)\mathbf{x}^H(t)$ and approximated from L samples using

$$\mathbf{R} \approx \hat{\mathbf{R}} = \frac{1}{L} \sum_{l=1}^L \mathbf{x}(t_l)\mathbf{x}^H(t_l) \quad (4)$$

where t_l is the time that the l th sample is taken. $\mathbf{P}_{\mathbf{B}}$ is the linear operator given by

$$\mathbf{P}_{\mathbf{B}} = \mathbf{B}(\mathbf{B}^H\mathbf{B})^{-1}\mathbf{B}^H \quad (5)$$

which projects its argument into the column span of \mathbf{B} . “Tr” in (3) indicates the trace operator, which is the sum of the eigenvalues of the matrix argument, or equivalently, the sum of its diagonal elements. This approach is optimal in the sense that it is asymptotically unbiased and no other estimator yields lower variance when the model conditions are satisfied and the estimate of \mathbf{R} is perfect.

For the special case of $M = 1$, the ML estimator simplifies to

$$\arg \max_{\phi_1} \mathbf{b}^H(\phi_1)\mathbf{R}\mathbf{b}(\phi_1). \quad (6)$$

Note that the function to be optimized is the power output from the “conventional beamformer” (CBF), that is, the power output from a beamformer whose inputs are weighted and summed so as to maximize gain in a certain direction subject only to a norm constraint on the weights [7]. Hence this estimator, which shall be referred to as “ML₁,” is equivalent to estimating the AOA as the peak of the CBF-derived angle spectrum, generated by sweeping the beam across the field of view. Similarly, the ML estimators for $M > 1$ can be interpreted as multidimensional generalizations of CBF-based discrete AOA estimator. Since the performance of the CBF is highly dependent on the array geometry and the incident signal distribution, it is clear that the performance of the ML estimator must also be dependent on these factors.

III. ARRAY GEOMETRIES

As indicated above, the array geometry is a factor in AOA estimation performance. However, the issue of array geometry has received very little attention in the past. Hua *et al.* [8] compares the Cramer–Rao Bound (CRB) for 2-D AOA estimation performance of several arrays, including an “L”-shaped array and a “+” (cross)-shaped array. The CRB gives a lower bound on the variance which can be achieved by any unbiased AOA estimator, including ML. Because the effective physical aperture of the “L” is always larger than the “+,” the CRB is found to be significantly lower for the L array. Liang and Paulraj [9] address the relationship between array geometry and *range*, using basic signal-to-noise ratio (SNR) arguments. However, the concept is not developed beyond the application to coverage extension.

Consider the following desired properties of an array geometry for AOA measurement. First, the array geometry should have uniform performance over the field of view. In this study, the field of view is the complete 360° span in the azimuthal plane. It is desirable to keep the spacing between at least some of the elements at $\lambda/2$ or less, in order to avoid response vector ambiguities. It is also desirable to have as large a physical aperture as possible, in order to improve resolution. However, the space available for a base station array is typically limited to a few wavelengths at UHF frequencies. Also, the total number of antennas in the array must be aggressively minimized in order to bear the cost of the associated electronics. Finally, given the harsh and dynamic nature of the mobile radio environment, it is not desirable to mechanically rotate or translate the array to achieve this aperture.

AOA estimation research has traditionally focussed on the uniformly spaced linear array (ULA) and the uniformly spaced circular array (UCA). The ULA is popular because it is simple to analyze and maximizes the physical aperture given a fixed number of elements, albeit for the broadside direction only. A well-known drawback of the ULA is poor AOA estimation performance near endfire [10]. One explanation for this is that the effective physical aperture of a ULA goes to zero at endfire. For the same reason, the ability of the ULA to resolve closely

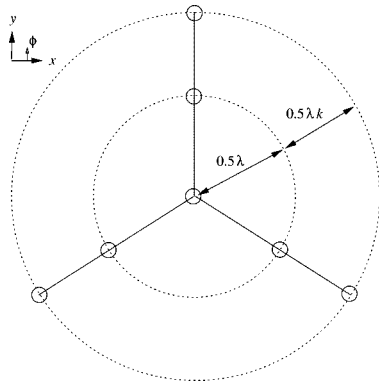


Fig. 1. Y array geometry. $k = 1$ for uniform spacing between elements on each leg.

spaced sources also severely degrades near endfire. These considerations rule out the ULA when consistent performance over a field-of-view of greater than 120° or so is desirable.

From this perspective, the UCA is an obvious candidate. The UCA has constant usable aperture as a function of azimuth. However, the UCA requires about twice as many elements to achieve the same usable aperture as the ULA at broadside. Since it is usually desired to use a dedicated receiver for each antenna element, the system cost is proportional to the number of elements. Thus, the UCA is a relatively expensive alternative in practice.

The Y geometry, shown in Fig. 1, is proposed as a less costly alternative. The Y is mentioned in [11] as a subarray concept; that is, as an option for selecting a small set of elements out of a much larger array for further processing. No justification or evaluation of this geometry is provided. The Y has also appeared in recent array signal processing papers by Gönen and Mandel [12], [13]. In [12], it simply serves as a test geometry for a blind copy algorithm. In [13], the Y is formed by augmenting an existing ULA with two additional uncalibrated linear arrays, intended in this case as a test geometry for AOA estimation with a mix of calibrated and uncalibrated subarrays.

To demonstrate the advantages of the Y with respect to some other popular geometries, several aspects of performance will be considered. First, there is the important issue of cost. To compare array geometries fairly, it is desired to know the cost per “unit of performance.” As indicated above, system cost is approximately proportional to the number of elements N . Performance can be quantified as proportional to the usable aperture Q , that is, the physical aperture that can actually be applied to a specific AOA estimation problem. Note that Q , in general, varies with ϕ . A reasonable cost metric is N/Q , that is, the number of elements required per unit of useful aperture. For some popular array geometries and the Y, one finds that

$$N/Q = \begin{cases} \frac{N}{N-1} |\cos \phi|^{-1}, & \text{for the ULA} \\ \pi, & \text{for the UCA} \end{cases} \quad (7)$$

$$\begin{cases} \frac{2N}{N-1} (|\cos \phi| + |\sin \phi|)^{-1}, & \text{for the L} \\ \frac{1.73N}{N-1} \leq N/Q \leq \frac{2N}{N-1}, & \text{for the Y.} \end{cases} \quad (9)$$

$$\frac{1.73N}{N-1} \leq N/Q \leq \frac{2N}{N-1}, \quad \text{for the Y.} \quad (10)$$

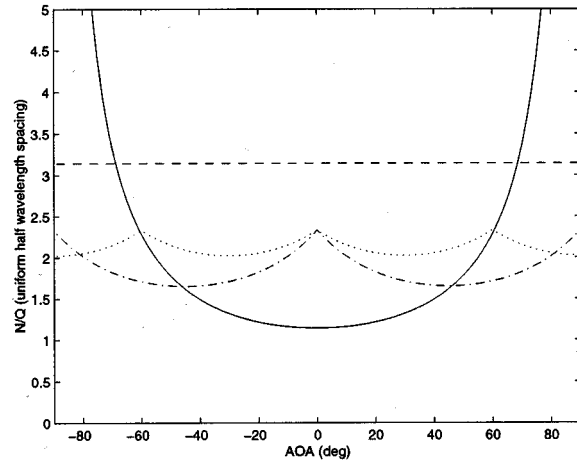


Fig. 2. Normalized cost-per-aperture ratio (N/Q). Solid: ULA ($N = 8$), Dash: UCA, Dash-dot: L ($N = 7$), Dot: Y ($N = 7$).

Above, the ULA is assumed to be oriented such that broadside is at $\phi = 0$; for the “L”-shaped array, one leg points along $\phi = 0$ and the orientation of the other leg is $\pm 90^\circ$. Q is figured in half-wavelength units. Also note that the expression for the UCA is a “large N ” approximation; in fact, N/Q for the UCA is higher for finite N . Finally, note that N/Q for the Y has 60° symmetry, so the limits given above are achieved every 60° . A plot of the above results is shown in Fig. 2. Note that the Y has a lower overall normalized cost than the UCA and is superior to the ULA for $|\phi| > 60^\circ$ or so. The L is slightly better for most angles, but the Y exhibits less variation over the field of view.

A further discriminator between the L and Y geometries is the avoidance of “endfire orientations,” that is, AOAs for which multiple elements fall in a line along the AOA. Elements in endfire are less helpful in AOA estimation; as mentioned above, the CRB for a linear array in endfire is infinite. The L geometry allows four elements to be placed in endfire simultaneously, which occurs when the AOA is 0° , 90° , 180° , or 270° . For the Y, no more than three elements can be placed in endfire simultaneously, corresponding to AOAs 90° , 210° , and 330° . For this reason, the Y was selected over the L in this study.

Now, let us consider only the Y and the ULA. A rigorous approach to comparing the relative AOA estimation performance of these geometries would be to explicitly compute the CRBs in each case. A suitable formulation of the CRB, which is applicable to arbitrary geometries, is given in [14]. In mobile radio applications, however, the SNR is typically greater than 10 dB and it is usually feasible to obtain $L > 10^2$ samples. A rough estimate of the CRB in this case is $6(N^3 \cdot \text{SNR} \cdot L)^{-1}$ [14], which corresponds to a root mean square error (RMSE) which is several orders of magnitude less than 1° . In mobile radio applications, real-world model errors such as angle spread and non-white noise covariance lead to much larger variances than predicted by the CRB. For this reason, let us consider a simpler approach. Recall that the ML_1 estimator is equivalent to finding the peak of the CBF power spectrum. Thus, insight into the performance of the ML estimator can be gained by considering the CBF pattern functions. To further simplify the analysis, let us assume $\mathbf{b}(\phi) \approx \mathbf{a}(\phi)$, i.e., the effect of mutual coupling is small. (This is justified in Section V.) CBF patterns for an $N = 8$ ULA

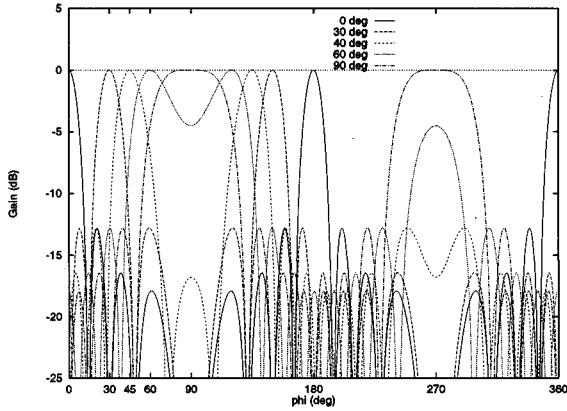


Fig. 3. Gain patterns of the eight-element ULA for various main beam pointing directions. Broadside is 0° .

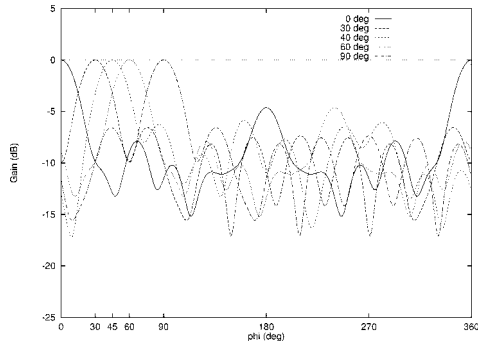


Fig. 4. Gain patterns of the seven-element Y array with $k = 1$ for various main beam pointing directions.

are shown in Fig. 3. Note the front-to-back ambiguity. Also note that the beamwidth widens toward endfire ($\pm 90^\circ$), and the main beam becomes distorted toward endfire. At broadside, the main beam half-power beamwidth (HPBW) is 14° ; at $\pm 60^\circ$ it has degraded to 29° . In the presence of noise, the AOA estimation variance increases with increasing beamwidth. Thus, it is clear that the ULAs AOA estimation variance degrades quickly beyond 60° . The same test is shown for the seven-element Y array in Fig. 4. In this case, the HPBW $\approx 30^\circ$ for all directions. The CBF beamwidth of the Y is greater than that of the ULA inside $\pm 60^\circ$, because there is one less element and two of the remaining elements do not contribute to widening the aperture. Therefore, the AOA estimation variance of the ULA is superior to that of the Y in that region of the field of view. However, the situation is reversed beyond 60° . Furthermore, the AOA estimation variance of the Y remains the same to 90° and beyond.

Taking into account both AOA estimation variance and cost, it is clear that the Y geometry is a good overall choice for systems requiring uniform performance over a field of view larger than 120° .

IV. ELEVATION PLANE DESIGN

Mobile communications antennas are typically vertically polarized (e.g., for vehicle rooftop use) or are intended to be used in a manner that favors vertical polarization (e.g., hand-held radios). Therefore, if the base station is limited to one polarization, it should be vertical. A natural choice for an array element in this

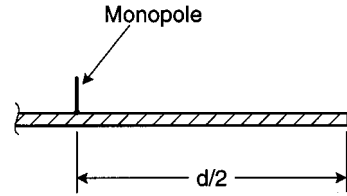


Fig. 5. Geometry for a monopole on a ground plane with "knife-edge" termination.

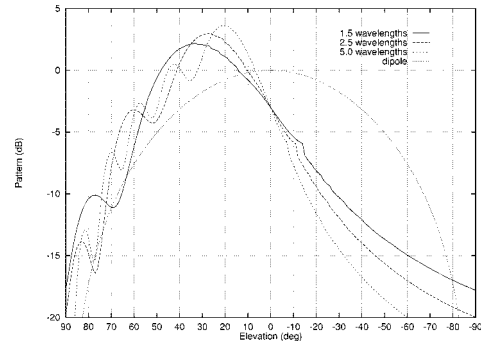


Fig. 6. Pattern of a quarter-wave monopole mounted on a ground plane with an edge at the indicated distances from the monopole.

case is a vertical dipole. However, a concern for AOA measurement is that the scattering and interference local to the array may corrupt the results. Since a vertical dipole has significant gain levels at low elevations, it may not be a good choice. An array of end-fed collinear dipoles can be used to narrow the elevation pattern; however, this approach may not yield sufficient suppression at low elevations. To strongly suppress local scattering and interference, it is proposed to design the array using monopoles on a ground plane. A ground plane can provide a hard shadowing of signals scattered directly from the mounting structure or scattered from locations which are too close to the array to be interpreted correctly as azimuth-only AOA's. This approach also leads to an antenna with a very low profile.

While it is obvious that a ground plane should provide deep suppression of signals arriving from directly below the array, the ground plane also affects the elevation pattern close to the horizon. In fact, truncation of the ground plane significantly reduces gain close to the horizon, where the desired signals originate. This unfortunately reduces the effective range of the system but may be preferable to the possibility of misleading results due to spurious local signals.

To illustrate the tradeoff between low-elevation suppression and horizon gain, an analysis of the pattern for a monopole on a ground plane, as shown in Fig. 5, was performed using the uniform geometrical theory of diffraction (UTD) [15]. Results are as shown in Fig. 6. Here, the elevation plane pattern is plotted and compared to a half-wave dipole in free space. Note that the close-in coverage for the monopole is greatly attenuated with respect to the dipole. However, note that the monopole pattern is 3 dB below the dipole at the incident shadow boundary (in this case, the horizon) regardless of the distance between the edge of the ground plane and the monopole. Thus, this configuration is not as good as a dipole in the primary coverage zone, corresponding to elevations between zero and -10° or so.

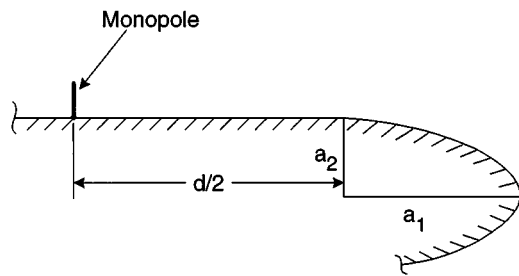


Fig. 7. Geometry for a monopole on a ground plane with an elliptical rolled edge termination.

A remedy for this problem is to terminate the edge of the ground plane using an elliptical rolled edge, as shown in Fig. 7. The rolled edge is attached with its semimajor axis parallel to the ground plane, such that the surface normal is continuous. This greatly reduces the diffraction from the edge (now, a junction).

However, there will still be a discontinuity in curvature across the junction, so diffraction may still be significant. Furthermore, a creeping wave mechanism is now present, which will increase gain for low elevation angles. The theory described in [15] cannot be used to evaluate performance in this case, as it does not apply to convex surface scattering. Pathak *et al.* developed a solution for convex surface scattering in [16]; however, this solution does not apply to surfaces which have a discontinuity in surface curvature. In [17], Pathak *et al.* presented a diffraction coefficient for a discontinuity in surface curvature; however, this solution does not account for the creeping wave. A method for calculating the pattern which is applicable to the scenario in Fig. 7 was suggested by Heedy and Burnside [18]. Their method uses the latter diffraction coefficient with the former convex surface scattering solution along with a correction factor to ensure the continuity of fields across the shadow boundary. This heuristic approach shows good agreement with a hybrid UTD/moment method technique developed by Chuang and Burnside for the analysis of “aperture matched” horns [19], [20]. Since the geometry of that problem is very similar to this geometry, it seems reasonable to apply the method of Heedy and Burnside here.

Using this formulation, the pattern of a monopole radiating in the presence of a ground plane terminated on one side by an elliptical rolled edge was evaluated, with results as shown in Fig. 8. Note that the primary zone gain is now *better* than the dipole, regardless of the rolled edge used. The close-in attenuation is also superior to the dipole.

The elliptical termination with parameters $a_1 = a_2 = 5.00\lambda$ is a circular rolled edge of radius 5λ . The elliptical termination with parameters $a_1 = 2.32\lambda$ and $a_2 = 1.08\lambda$ is designed to have a radius of curvature of 5λ at the junction point (same as the 5λ circular rolled edge) and 0.5λ at the extreme end. Note that this rolled edge has performance which is nearly identical to the 5λ circular rolled edge for elevations within 40° of the horizon. Furthermore, the performance of these rolled edges is not sensitive to the distance between the monopole and the junction point.

To show the effect of further reduction in the size of the elliptical rolled edge, Fig. 8 also shows the result for an elliptical termination with parameters $a_1 = 1.26\lambda$ and $a_2 = 0.79\lambda$. This

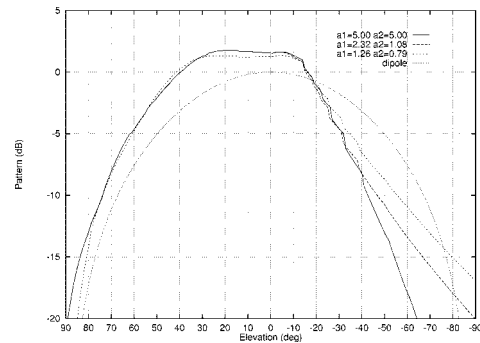


Fig. 8. Pattern of a quarter-wave monopole mounted 1.5λ from the junction between a ground plane and various elliptical terminations.

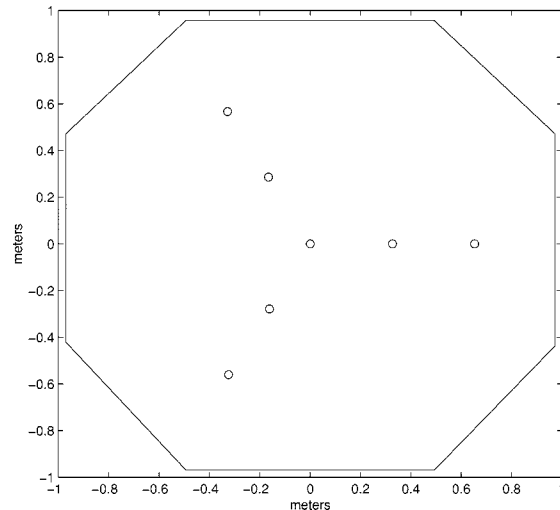


Fig. 9. Top view of array geometry. The circles indicate monopole positions and the outline of the ground plane is indicated. As built, the top edge of this figure is North.

rolled edge has a radius of curvature of 2λ at the junction point. Note that the degradation is small.

V. MUTUAL COUPLING AND CALIBRATION

As indicated above, the mutual coupling among the elements in the antenna array influences the performance of an AOA estimator. Therefore it is of interest to characterize the mutual coupling for the array design proposed above. This entails a computation of the open-circuit impedance matrix \mathbf{Z} . A reasonable technique to calculate \mathbf{Z} is the moment method [21]. The Electromagnetic Surface Patch code (ESP5) is a particularly convenient moment method tool [22]. In anticipation of the field study described below, a prototype “Y”-shaped array of quarter-wave monopoles was mounted on an unterminated ground plane as shown in Figs. 9 and 10. Each monopole is constructed from brass rod of length 157 mm (about one quarter wavelength at 465 MHz) and approximately 2 mm in diameter, and welded to the center conductor of a panel mount style “N” coaxial connector. The N connectors were mounted to a single section of aluminum sheet which forms the central portion of the ground plane. The ground plane was then extended to the dimensions indicated in Fig. 9 using aluminum screen material supported by a wooden frame. In ESP5, this antenna array was modeled as an arrangement of perfectly conducting plates and wires. ESP5



Fig. 10. Array as built. View is slightly North of East.

TABLE I
MAGNITUDE (dB) OF THE OPEN CIRCUIT IMPEDANCE MATRIX, NORMALIZED
TO THE SELF-IMPEDANCE OF THE CENTER ELEMENT

ELEMENTS	1	2	3	4	5	6	7
1	0.0	-7.5	-6.8	-6.9	-11.7	-11.8	-11.6
2		-0.6	-11.0	-10.8	-8.0	-14.9	-13.8
3			-0.7	-10.8	-14.4	-7.8	-14.2
4				-0.6	-15.6	-14.1	-7.7
5					-0.6	-16.4	-15.5
6						-0.7	-16.8
7							-0.7

*Elements are numbered as follows: center element is 1, inner elements are 2-3-4, and outer elements are 5-6-7. Arms of the Y are defined by 1-2-5, 1-3-6, and 1-4-7.

provides as output (among other things) its calculation of \mathbf{Z} . For the array described above, the magnitudes are given in Table I.

Table I shows that the mutual coupling is related to the distance between elements, as expected. The strongest coupling exists between adjacent elements along each arm of the array, and is about -7 dB. Other coupling coefficients range between -11 and -17 dB. Further analysis has shown that this result is not sensitive to the dimensions of the ground plane, as long as the edge is at least 0.5λ from the nearest monopole. Thus, this result also applies when the ground plane is terminated in a rolled edge.

This coupling is strong enough to significantly bias the AOA estimates; thus, neglecting coupling when computing trial response vectors for use in (3) may not yield accurate results. However, it may not be safe to assume that the coupling matrix inferred by the moment method is better. In a study of an 11×11 array of quarter-wave monopoles with half-wavelength spacing on a flat ground plane, Fenn [23] compared the multipoint scattering coefficients computed using a moment method solution to the same coefficients computed from measurements. He observed that the magnitudes in each case were in good agreement, but with a significant error in the phase. However, the phase errors were about the same for every coefficient. This was attributed to model assumptions in the moment method calculation, in particular, the nature of the monopole feeds and the

assumed current modes for each monopole. This phase discrepancy can also bias the ML estimator.

However, note that the impedance matrix is related to the scattering coefficients by

$$\mathbf{S} = (\mathbf{Z} - \mathbf{I})(\mathbf{Z} + \mathbf{I})^{-1} \quad (11)$$

which assumes \mathbf{Z} has been normalized by the feedline characteristic impedance. Thus, the *desired* value of \mathbf{Z} may differ from the computed value only in a single parameter, namely, the phase of the associated scattering coefficients.

A simple method to exploit this observation is as follows. One can measure the array output due to sources at various sites distributed over the field of view. The AOA is estimated in each case and compared to the true bearing to determine the estimation bias. The desired coupling matrix is then the one which minimizes the overall variation among the biases. Ideally, the optimal value of the phase parameter would reduce the bias for each of the test sites to zero. However, it is possible that there is some error in the orientation of the array. In other words, the element positions may be known exactly with respect to other array elements, but the array itself may be rotated by some previously undetected amount. In this case, the optimal phase parameter is that which yields the smallest variation around some constant bias, and this bias is an estimate of the orientation error. Results obtained using this technique in field conditions are presented below.

VI. FIELD MEASUREMENTS

This section describes the results of a field experiment used to confirm the azimuthal AOA estimation performance of the array shown in Figs. 9 and 10. The experiments were performed in November 1999 on the west campus of the Ohio State University.

A. Experiment Design

The antenna array was mounted on the roof of the three-story ElectroScience Laboratory (ESL) building, with the ground plane approximately 10 m above ground level, as shown in Fig. 10. In this case, the ground plane is essential in suppressing interference from within the building and also scattering from various other structures on the roof. The transmitter is an unmodified commercially available handheld radio carried by a person on foot. The radio transmits 500 mW at 462.6625 MHz using analog FM modulation of about 12.5-kHz bandwidth. For each trial, 3025 samples are acquired using a self-calibrating coherent array receiver developed at ESL. The trials are separated in time by about 25 s.

At each site, the user was instructed to talk normally into the radio. To obtain a more representative distribution of local fading conditions, the user was also instructed to walk in a circle of diameter 6 m ($\approx 9\lambda$) while transmitting. The channel coherence time in this situation is at least 20 ms; therefore, the scenario is effectively stationary over the 802- μ s acquisition time. No special attempt was made to hold the radio to maintain any particular polarization; in fact, it was observed that most users tended to hold the radio in a position about halfway between

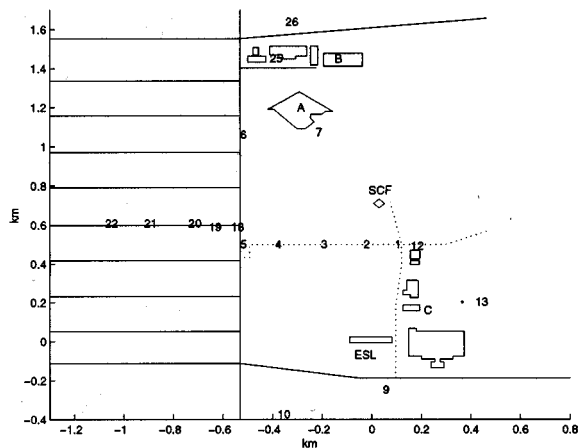


Fig. 11. Test Area. The right edge faces East (0°), and the top edge faces North (90°).

vertical and horizontal polarization. Because the handheld’s antenna has a dipole-like pattern, and the user is walking in circles, the SNR at the array tends to vary over a few decibels from acquisition to acquisition, even in line-of-sight (LOS) conditions.

B. Test Area

The test area is illustrated in Fig. 11, with the test sites identified by number. A total of nine transmit sites were selected for this evaluation. The location of each site is known to within about 10 m, which means the true bearing measured from the array site to the closest test site (about 500 m away) is known to within $\pm 1.2^\circ$. To the north of the array site is a large open field. This field is bordered on the west by a two-lane road with single-family homes and to the north by a four-lane road with single-level small business offices. A very large four-story office building, which shall be called “Building A,” is located at the northwest corner of the field. Building A spans about 11° of the field of view as seen from the array site. “Building B” is a bowling alley which extends another 7° beyond the east edge of Building A. To the northeast is a cluster of industrial buildings, including “Building C,” a prominent 30-m high structure that spans about 4° . Also in the north field is a small building identified as the Satellite Communications Facility (SCF). Immediately south of the array site is a two-lane road; across this road is an apartment complex consisting mainly of two-story townhouses.

C. Calibration Results

Calibration of the antenna array was performed using the technique described in Section V. Data was collected while the mobile was transmitting from Sites 2–7, which are uncluttered and have line-of-sight to the array. Data collected from regions to the east and south of the array were not included in the calibration process due to the inability to obtain uncluttered transmit sites with clear LOS. Separately, an estimate of the open-circuit impedance matrix was computed using ESP5. Using the ML_1 estimator, the matrix Z was found which minimized the variation in the bias of one AOA estimate from each of the six sites.

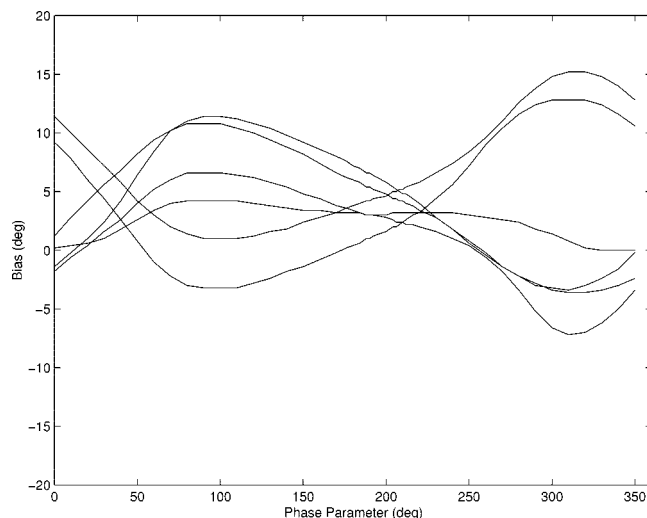


Fig. 12. Bias for each of six acquisitions (corresponding to Sites 2–7) as a function of the impedance matrix phase parameter.

The block of data selected to represent each site was chosen on the basis of highest SNR.

Using $Z = I$ (no calibration), the bias varied between 2.4° to 6.6° , for a total range of 4.2° . The results of the calibration procedure are shown in Fig. 12. Using the ESP5 solution with phase parameter equal to 0° , the bias varied between -1.8° to 11.4° . Using the optimum phase parameter of 210° , the observed biases are limited to $3.7^\circ \pm 1.4^\circ$. Subsequent examination of the array revealed that it was in fact installed off-center by about 3° , which fortunately could be accounted for in the post-processing. The results shown in the next section reflect this correction. The apparent second point of minimum variation near 50° is not valid, as it gives rise to response vectors (b) which are not consistent with far-field sources. From these results, it is inferred that the antenna array calibration contributes less than 2° of error to the bias measurements for sites between 90° and 135° azimuth.

D. AOA Estimation Results

To confirm the performance of the array, AOA measurements were made for Site 1, Sites 2–7 (to the north of the array, also used for calibration), and Sites 9 and 10 (to the south and west of the array). The results using the ML_1 estimator are shown in Table II. For Sites 1–7, the performance is reasonably good, with the bias generally being under 2° , which is well within the expected error range defined by the uncertainty in the true position as noted above. For Sites 9 and 10, the bias is slightly higher. One possible explanation is that this region was not represented in the array calibration procedure. However, these sites are in cluttered surroundings with an obstructed line-of-site; thus it may also be that this data, as opposed to the geographical line of bearing, actually represents the true AOA.

The variance, expressed in terms of the root mean square error (RMSE), is also shown in Table II. The RMSE is on the order of 2° or less, except for Sites 1 and 9, which are much higher. The CRB, assuming the model conditions stated earlier, is 2 to 3 orders of magnitude less than the RMSE observed. The observed RMSE is much greater than the CRB due to a combination of

TABLE II
AOA MEASUREMENT PERFORMANCE USING ML_1

SITE	RANGE	BEARING	TRIALS	MEAN SNR	BIAS	RMSE
1	0.5 km	76°	26	27 dB	+0.6°	6.1°
2	0.5 km	90°	6	32 dB	+1.8°	2.1°
3	0.5 km	109°	5	30 dB	+1.3°	1.0°
4	0.6 km	126°	6	31 dB	-0.3°	1.2°
5	0.7 km	135°	22	27 dB	-1.6°	2.1°
6	1.2 km	115°	9	20 dB	+0.6°	1.9°
7	1.1 km	100°	6	25 dB	+0.9°	1.1°
9	0.2 km	287°	8	32 dB	-3.6°	10.2°
10	0.5 km	227°	12	29 dB	+3.3°	2.3°

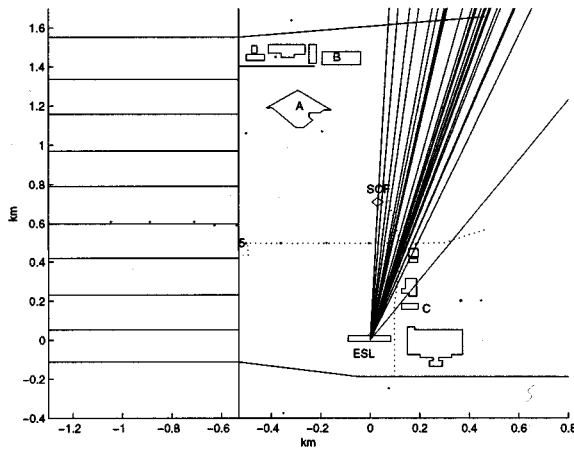


Fig. 13. AOAs estimated for Site 1 using ML_1 .

factors, including model errors. Important model errors in this experiment include angle spread due to complex scattering and colored noise covariance due to subtle differences among the receivers.

To better understand the results for Site 1, this data was further analyzed using the ML estimator with $M = 2$, i.e., assuming two incident signals. This estimator is referred to as ML_2 . Fig. 13 shows the AOAs estimated by ML_1 for Site 1. Figs. 14 and 15 show the first and second AOAs estimated by ML_2 , respectively, from the same data. The joint AOA distribution from ML_2 is shown in Fig. 16. Two types of behavior are evident. One cluster of AOA pairs shows a first AOA close to the true line of bearing and a second AOA in the range 93° – 110° . As shown in Figs. 15 and 16, the distribution of the second AOA in this case strongly suggests that it is mainly due to scattering from Buildings A and B, with intermittent scattering from the SCF and various buildings on the east and west sides of the field. It is not surprising that different scattering occurs at each trial, since the mobile transmitter is moving and the environment is expected to display “fast” fading conditions with Rayleigh or Ricean behavior. For this site, increasing the model order from 1 to 2 reduces the RMSE for the first AOA from 6.1° to 5.0° , which can also be observed as the tighter clustering of AOA estimates in Fig. 14 as opposed to Fig. 13.

The second cluster of AOA pairs shown in Fig. 16 shows very low variance for the first AOA and with a second AOA of

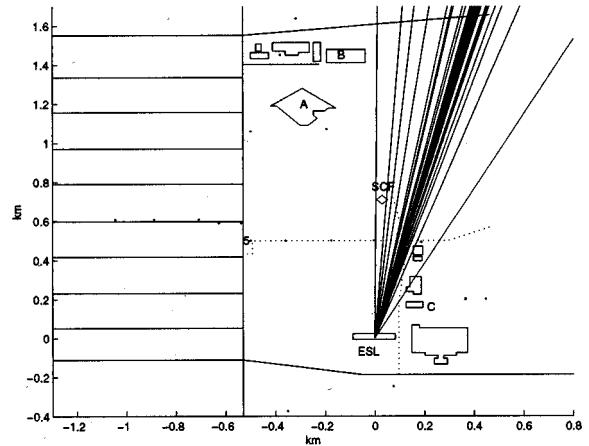


Fig. 14. AOAs estimated for Site 1; ML_2 , first AOA.

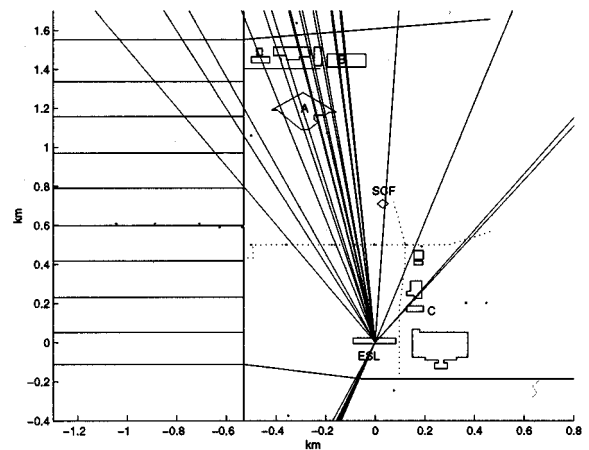


Fig. 15. AOAs estimated for Site 1; ML_2 , second AOA.

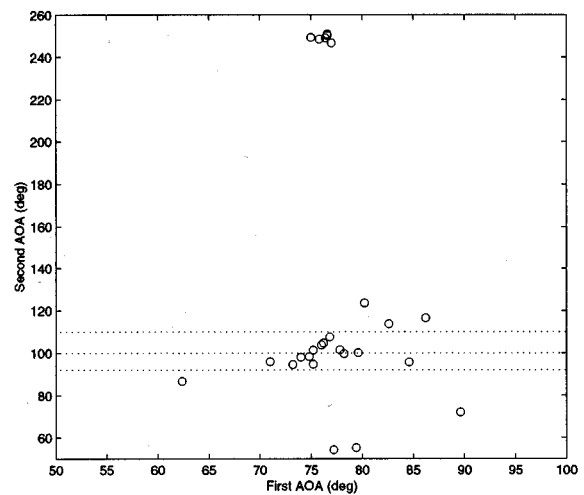


Fig. 16. Joint distribution of AOAs estimated for Site 1 using ML_2 . The dashed lines indicate the optical boundaries of west and east edges of Building A (top and middle lines, respectively) and the east edge of Building B (bottom line).

about 250° . No terrain feature can be associated with this second AOA. Therefore, it is believed to be spurious in the sense that the best M for those trials may actually be 1.

VII. CONCLUSIONS

This paper described a novel antenna array concept which uses a “Y”-shaped distribution of quarter-wave monopoles on a ground plane to achieve uniform coverage in the azimuth, with greatly reduced potential for scattering from nearby structures and interference from low elevation angles. A simple method for field calibration of this array was developed. A prototype of this array has been built and tested in field conditions at 460 MHz. Using ML estimation, it was shown that the array system is able to resolve single AOAs to within a few degrees and is able to identify discrete multipath as well. A shortcoming of the field-tested design is that it has poor gain along the horizon, due to diffraction from the edge of the ground plane. To control this diffraction, an elliptical rolled edge termination was proposed. Using a rolled edge, the horizon gain can be increased by 5 dB while maintaining high suppression at low elevations. Taking the array factor into account, this array can achieve gain comparable to the stacked dipole configurations traditionally used at base stations. Furthermore, this performance can be achieved in an antenna system which is about one wavelength in height, including the rolled edge.

ACKNOWLEDGMENT

The author gratefully acknowledges the helpful comments of Prof. W. D. Burnside, Dr. I. J. Gupta, Prof. R. L. Moses, and Prof. E. H. Newman. P. Diez and J. Hetrick assisted in the field measurements.

REFERENCES

- [1] A. Paulraj and C. Papadias, “Space-time processing for wireless communications,” *IEEE Signal Processing Mag.*, pp. 49–83, Nov. 1997.
- [2] R. Ertel *et al.*, “Overview of spatial channel models for antenna array communication systems,” *IEEE Personal Commun. Mag.*, pp. 10–22, Feb. 1998.
- [3] T. Rappaport, J. Reed, and B. Woerner, “Position location using wireless communications on highways of the future,” *IEEE Commun. Mag.*, pp. 33–41, Oct. 1996.
- [4] J. Kennedy and S. Ellingson, “Smart antenna testbed for mobile wireless systems,” in *Proc. Virginia Tech’s Sixth Symp. Wireless Communications*, Blacksburg, VA, June 1996.
- [5] P. Mogensen *et al.*, “Preliminary measurement results from an adaptive antenna array testbed for GSM/UMTS,” in *Proc. 47th IEEE Vehicular Technology Conf.*, Phoenix, AZ, May 1997.
- [6] I. Ziskind and M. Wax, “Maximum likelihood localization of multiple sources by alternating projection,” *IEEE Trans. Acoust., Speech, Signal Processing*, vol. 36, pp. 1553–1560, Oct. 1988.
- [7] S. Pillai, *Array Signal Processing*. New York: Springer-Verlag, 1989.
- [8] Y. Hua, T. Sarkar, and D. Weiner, “An L-shaped array for estimating 2-D directions of arrival,” *IEEE Trans. Antennas Propagat.*, vol. 39, pp. 143–146, Feb. 1991.
- [9] J.-W. Liang and A. Paulraj, “On optimizing base station antenna array topology for coverage extension in cellular radio networks,” in *Proc. IEEE Vehicular Technology Conf.*, 1995, pp. 366–370.
- [10] S. Kay, *Fundamentals of Statistical Signal Processing: Estimation Theory*. Englewood Cliffs, NJ: Prentice-Hall, 1993.
- [11] H. Alnajjar and D. Wilkes, “Adapting the geometry of a sensor sub-array,” in *Proc. ICASSP*, vol. IV, 1993, pp. 113–116.
- [12] E. Gonen and J. Mendel, “Application of cumulants to array processing—Part III: Blind beamforming for coherent signals,” *IEEE Trans. Signal Processing*, vol. 45, pp. 2252–2264, Sept. 1997.
- [13] —, “Application of cumulants to array processing—Part IV: Direction-finding in coherent signals case,” *IEEE Trans. Signal Processing*, vol. 45, pp. 2265–2276, Sept. 1997.
- [14] P. Stoica and A. Nehorai, “Music, maximum likelihood, and cramer-rao bound,” *IEEE Trans. Acoust., Speech, Signal Processing*, vol. 37, pp. 720–741, May 1989.
- [15] R. Kouyoumjian and P. Pathak, “A uniform geometrical theory of diffraction for an edge in a perfectly conducting surface,” *IEEE Trans. Antennas Propagat.*, vol. 62, pp. 1448–1461, Nov. 1974.
- [16] P. Pathak, W. Burnside, and R. Marhefka, “A uniform gtd analysis of the diffraction electromagnetic waves by a smooth convex surface,” *IEEE Trans. Antennas Propagat.*, vol. AP-28, pp. 631–642, Sept. 1980.
- [17] P. Pathak, C. Chuang, and S. Shrikanth, “Joint services electronics program fifth annual report,” The Ohio State University ElectroScience Lab., Technical Rep. 710 816-12, Dec. 1982.
- [18] D. Heedy and W. Burnside, “An aperture-matched compact range feed horn design,” *IEEE Trans. Antennas Propagat.*, vol. AP-33, pp. 1249–1255, Nov. 1985.
- [19] W. Burnside and C. Chuang, “An aperture-matched horn design,” *IEEE Trans. Antennas Propagat.*, vol. AP-30, pp. 790–796, July 1982.
- [20] C. Chuang and W. Burnside, “A diffraction coefficient for a cylindrically truncated planar surface,” *IEEE Trans. Antennas Propagat.*, vol. AP-28, pp. 177–182, Mar. 1980.
- [21] J. Kraus, *Antennas*, 2nd ed. New York: McGraw-Hill, 1988.
- [22] E. Newman, *A User’s Manual for The Electromagnetic Surface Patch Code: Preliminary Version ESP5.0*: The Ohio State University ElectroScience Lab., 1998.
- [23] A. Fenn, “Theoretical and experimental study of monopole phased array antennas,” *IEEE Trans. Antennas Propagat.*, vol. AP-33, pp. 1118–1126, Oct. 1985.
- [24] J. H. Reed, B. D. Woerner, and T. S. Rappaport, Eds., *Wireless Personal Communications: Advances in Coverage and Capacity*. New York: Kluwer, 1997.

Steven W. Ellingson (S’87–M’90) received the B.S. degree in electrical and computer engineering from Clarkson University in 1987, and M.S. and Ph.D. degrees in electrical engineering from the Ohio State University in 1989 and 2000, respectively.

Since 1997, he has been a Research Scientist with the Ohio State University ElectroScience Laboratory. From 1995 to 1997, he was a Senior Systems Engineer with Raytheon E-Systems, Falls Church, VA. From 1993 to 1995, he was a Senior Consultant with Booz-Allen and Hamilton, McLean, VA. From 1989 to 1993, he served on active duty with the U.S. Army, reaching the rank of Captain. His research interests include array signal processing, interference suppression, and RF system design.